# Flow patterns and heat transfer coefficients using a rotational diffuser coupled with a radiant floor cooling.

Francisco Fernández-Hernández[1], Alberto Fernández-Gutiérrez[2], Juan José Martínez-Almansa[2], C. del Pino[2] and L. Parras[2]

[1]Universidad de Málaga, Escuela de Ingenierías Industriales, Energy Research Group, C/ Doctor Pedro Ortiz Ramos s/n; 29071 Málaga (Spain)

[2]Universidad de Málaga, Escuela de Ingenierías Industriales, C/ Doctor Pedro Ortiz Ramos s/n; 29071 Málaga (Spain)

## Abstract

In this research, we explore the characteristics of one HVAC system integrated by a rotational floor diffuser with an underfloor plenum, coupled with a radiant floor cooling. Numerical simulations are performed using two different meshes. On the one hand, the diffuser outflow entering into the room using a very detailed mesh. On the other hand, the whole room with the radiant floor through the outflow obtained from the former diffuser mesh. Besides, we collect the experimental shape of the plume near the rotational diffuser from smoke visualizations. We show that there exist two different regimes depending on the flow rate. Firstly, displacement ventilation, and secondly, a very active mixing process for low or high flow rates, respectively. We compute the Nusselt number against Reynolds number, and they collapse in a linear fitting with two different slopes below and above Reynolds number 15000. Hence, the type of flow patterns created near the diffuser only affect the level of heat transfer, but not its linear dependency. Finally, we propose another general non-linear fitting of the Nusselt number as a function not only of Reynolds number but temperature differences for all the cases considered (isothermal and non-isothermal). This latter fitting shows us that only inertia controls heat transfer.

## 1. Introduction

Heating, ventilation and air conditioning (HVAC) technology is in continuous progress to improve thermal comfort, reduce energy consumption, and guarantee good air quality in buildings [1-6]. In this way, the performance of the combination of an underfloor air distribution system (UFAD) with a radiant floor is proposed and analyzed in this paper.

Unlike a traditional overhead system, in UFAD systems supplying fresh air by a plenum near the floor implies the displacement ventilation (DV) method. Hence, fresh air is pushed to the zone at low velocity, and it is warmed up by heat sources in the room, and finally exhausted with the contaminants by buoyant forces using a return system near ceiling level. Nevertheless, when fresh air from the diffuser has significant vertical momentum, DV becomes a mixing ventilation (MV) device that is characteristic of conventional ceiling-based air distribution (CBAD) systems. The advantages of UFAD against CBAD systems are well known: indoor air quality [2], thermal comfort [3], layout flexibility [4,5], and improved energy efficiency due to a thermal stratification by a floor-to-ceiling airflow pattern [1,6].

On the other hand, radiant cooling systems are increasingly used for its energy efficiency and enhanced thermal comfort, despite some weaknesses as the limitation of the cooling capacity due to the possibility of condensation on the floor, the high thermal inertia or the requirement of a complementary ventilation system to guarantee the inlet of fresh air. For these reasons, the combination of a radiant floor cooling and a forced ventilation system could solve these disadvantages. Atienza et al. [7] raise several control strategies in a hydronic heating system that combines two different terminal units, radiant floor, and fan-coil, in the same thermal zone. Also, some studies on cooling systems in suited spaces for UFAD systems as high heights, high internal gains by occupants, etc., found that radiant floor cooling can improve both indoor thermal comfort and system energy efficiency compared with a convective CBAD cooling system [8].

The complexity of the combined system that requires additional space for the air-handling unit, the ductwork, and the air diffusers limits a more extensive use. As a solution, Fernández et al. [9] and Atienza et al. [10] proposed a new system that integrates a radiant floor and a UFAD system in the same terminal unit. It consists of polypropylene with wood fiber modular floor panels installed above the structural slab of the building. The air ventilation flows through the void space used as a plenum, and in the upper face of the module, the radiant floor pipes are installed in a typical layout (spiral, serpentine, etc.), and are embedded in a concrete layer. Above, the surface finish of marble, tile, wood, among other types of materials, is added with diffusers distributed by the floor. Consequently, this system enables punctual air supply using floor diffusers together with a control of the floor temperature, setting desired temperature differences between air and basement, while with a conventional UFAD system this is not possible to achieve. In both papers [9-10], a numerical and experimental study is performed, and the novelty and conclusions of them are related to a thermal analysis of thermal decay, evaluate the potential cooling capacity of the unit and check the thermal comfort is achieved by means of the operative air temperature.

Several authors have investigated the experimental and numerical analysis of UFAD and DV systems. Zhang et al. [11] highlighted how the thermal stratification in the room was substantially determined by the outlet velocity of the plenum. Analogously, Raftery et al. [12] performed 19 full-scale laboratory experiments with a variation of the number of diffusers and the internal loads for the measurement of the level of thermal stratification. Besides, Yau et al. [13] examined the geometrical effect of the floor swirl diffuser regarding the airflow pattern by means of smoke tests visualizations and CFD analysis. Based on the experimental technique two-dimensional Particle Image Velocimetry (2D-PIV), Li et al. [14] analyzed the airflow pattern of a UFAD system and its influence in human comfort.

Nevertheless, how affects the presence of a radiant cooling floor in UFAD systems is not yet analyzed because of the complexity of the combined system. Causone et al. [15] showed how heating or cooling floor affects mainly to the temperature and velocity air profiles with a DV system using a wall diffuser, and Raftery et al [16] combines an UFAD system with a cooled radiant ceiling slab and shows a 22–23% reduction in total energy consumption during the peak cooling months comparing with a typical overhead

system. Finally, in a small-scale experimental tests, Fernández-Gutierrez et al. [17] use radial diffuser with a cooling floor, and they obtained experimentally and numerically a correlation for Nusselt as a function of Reynolds and Grashof numbers taking into account a logarithmic function of the non-dimensional radial distance of the diffuser together with the associated flow patterns.

Therefore, the purpose of this paper is a numerical and experimental analysis of a new terminal unit that combines a radiant floor with a UFAD system. From the previous developed works [9-10], we consider that an additional CFD analysis (validated by experimental tests and smoke visualization of the jet) of the terminal unit is very important in order to obtain information about this new terminal unit which are not seen before, such as: study the interaction of the air supplied by a swirl floor diffuser coupled with a cooling radiant floor, evaluate the influence of flow patterns on heat transfer coefficients and how it is affected by a DV or MV, analyze the shape of the air jet supplied, visualize the movement of the air near the floor, measure the zone temperature stratification, etc. To this aim, in section 2, the experimental setup is described with detail and, besides, we present the theoretical model for the calculation of the convective heat transfer coefficient in the floor. Afterward, in section 3, a CFD study is performed using the open-source code OpenFOAM [18]. Finally, the results of the paper are presented in section 4, and we compare the experimental measurements with those obtained numerically, plus the correlation between Nusselt and Reynolds numbers to establish a comparison between DV and MV systems, which is very useful for engineers HVAC designers.

## 2. Experimental setup.

### *2.1 Description of the experiment.*

We describe the experimental setup unit that it is also the one used in Fernández et al. [9] and Atienza et al. [10]. The terminal unit has a floor area of 3x3 $m^2$ (like the assembly of 25 modular floor panels), and it has an underfloor air plenum of 8 cm height (Fig.1).

Fig. 1. The modular floor panel.

Over the plenum, the radiant floor layer is disposed, with polyethylene tubes (diameter: 16.2/20 mm and 13 cm of tube spacing) in reverse spiral return, embedded in a uniform concrete coating with a thickness of 3 cm, and placed over a rigid polyurethane foam insulation layer 2.5 cm thick. We have one Schako air diffuser model BDA-AK 200 at the center of the floor that pushes the air to the surrounding room that is mimic by a canvas tent of 2.5 m height. This device has a diameter of 200 mm and 24 vanes with two different sizes that impose the rotation to the main flow.

The whole system works as follows. Water is chilled or heated in the heat pump and flows through the pipes changing the floor temperature. Also, an air handling unit (AHU) cools or heats the air ventilation that is supplied by a circular duct to the ground plenum. The rotational diffuser is located in the center of the floor, so the airflow is pushed at low or high flow rates to the surrounding room as displacement or mixed ventilation, respectively. We also explain the cooling mode briefly. The radiant floor handles the maximum sensible load, limited by the condensation on the floor surface. Airflow ventilation removes the remaining sensible and latent loads, and the outside air ventilation is required to maintain the air quality. Fig. 2 shows a picture of the experimental unit with a legend of the different components.

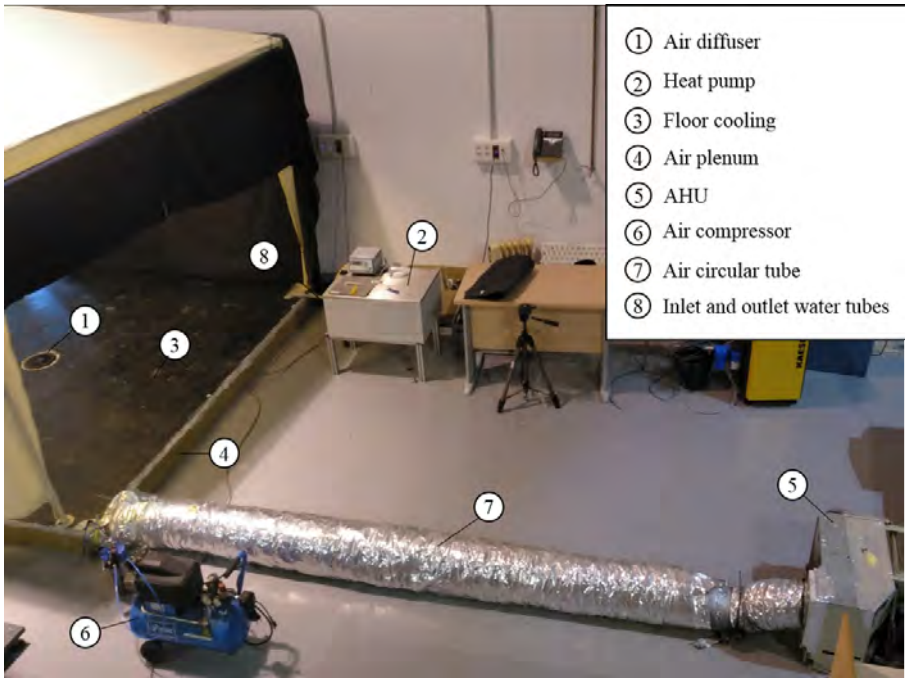


Fig. 2. The experimental unit that consists of: air diffuser (1), heat pump (2), floor cooling (3), plenum (4), AHU (5), air compressor (6), air circular tube, (7) and inlet/outlet water tubes (8).

The main aim of this terminal unit is to take advantage of the qualities of a UFAD system operating with a radiant floor. We carry out experimental tests to solve the uncertainties of the system performance corresponding to the shape of the thermal plume of the supplied air to the surrounding room as a function of the airflow rate or the presence of a cooling floor with different temperatures imposed. To start with, we describe the monitoring of the terminal unit below.

We measured air room temperature to check the temperature stratification using thermal sensors type Hobo U12, which are located at different heights (5 cm, 90 cm, 120, and 160 cm). Also, a globe thermometer measures the operative temperature. It consists of a black hollow sphere made of copper, with a diameter of 150 mm. The measurement range of this device is between 0 and 120ºC with an accuracy of a type K thermocouple, class 1. Besides, a temperature Hobo U12 is placed out of the zone to measure the surrounding temperature, see details in Fig. 3.

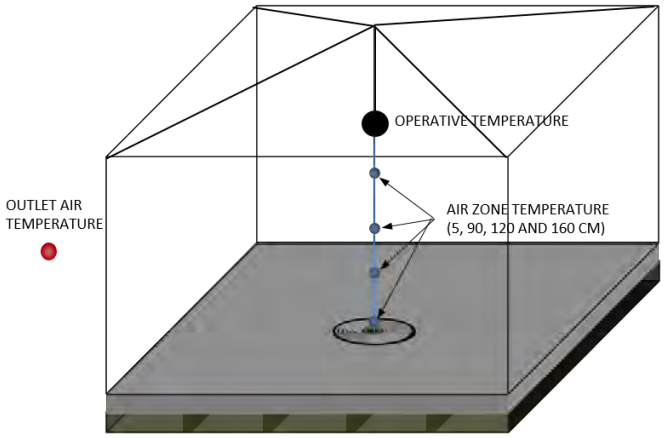


Fig. 3. Zone air temperature monitoring.

We also measured air ventilation temperature and velocity. The small air-handling unit, provided with a direct expansion coil and a variable speed fan, controls the temperature and the volume of air supplied to the zone. A hot-wire anemometer (Testo 480, range 0÷20 m/s), placed in the circular tube with an internal section of 0.029 $m^2$, at the entrance of the plenum, measures the air velocity. We assume that the flow is turbulent and fully developed inside the circular pipe. To estimate heat losses in the plenum (the thermal decay) we measured both the inlet in the plenum temperature and supply airflow in the rotational diffuser temperature with a Hobo U12 unit together with the associated flow rates. The influence of a cooling radiant floor layer above a plenum in the thermal decay has been discussed in [9, 10] and it is not an objective of this study.

On the other hand, it is essential to evaluate the performance of the radiant floor, especially in cooling mode, to prevent water condensation over the floor. We measured the surface floor temperature with four thermal sensors type Hobo U12, with a plated copper sensor probe (TMC6-HE) mounted onto the floor surface, see the 3D sketch in Fig. 4. The accuracy is ±0.25°C ranging between 0° and 50°C that are the values corresponding to our study. Two PT100 probes measure the temperatures of water as it enters and exits the radiant floor system. The accuracy is ±0.05°C in the range -80°C÷300°C. The water mass flow rate remains constant, and it is measured with a rotameter flow meter Geonica (range [0,650] l/h). The chilled water entering the floor comes from a PolyScience chiller of 2.3 kW.

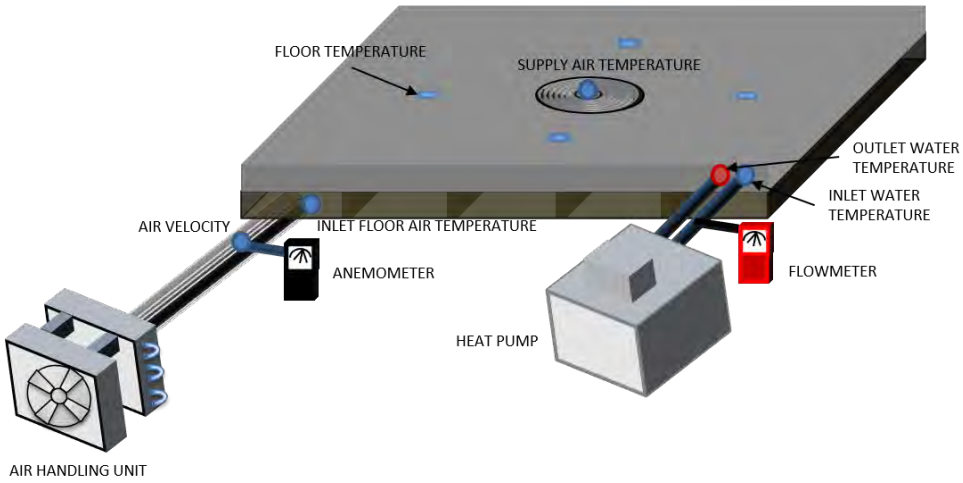


Fig. 4. The radiant floor and air ventilation monitoring.

To allow flow visualizations, we used a Laskin type smoke generator that produces a mixture of smoke and air [19]. The uniform mixing of particles with 1-micron diameter (which are non-intrusive) generates a smoke that is illuminated by a green laser Melles Griot of 2W. The laser sheet in a two-dimensional plane is produced using a cylindrical lens. We performed flow visualizations with a digital camera and post-processing the videos allow us to obtain different snapshots and the mean image over a period that is typically 30 seconds. Finally, Table 1 summarizes the sensors and its positions used in the experimental setup.

| Parameter | Measurement points | Vble | Instrument | Range of measures |
|---|---|---|---|---|
| Floor surface temperature | 4 points | $T_f$ | Thermal sensors Hobo U12, with TMC6-HE | 20-22ºC |
| Room air temperature | 4 points in heights (5, 90, 120 and 160 cm) | $T_z$ | Thermal sensors Hobo U12 | 25-28ºC |
| Operative temperature | 1 point in the centre of the room (170 cm height). | $T_{op}$ | Globe thermometer | 24-26ºC |
| Ventilation air temperature | 2 points in the plenum | $T_{sup}$ | Thermal sensors Hobo U12 | 15-22ºC |
| Volumetric air flow rate | 1 point entering in the plenum | $Q_{air}$ | Hot wire anemometer (Testo 480) | 75-250 $m^3/h$ |
| Water temperature | Supply and return water temperature | $T_w$ | PT100 probe (Testo) | 15-18ºC |
| Water mass flow rate | Supply water flow rate | $m_w$ | Flow meter (Geonica) | 0-650 l/h |

| | | | | | |
|---|---|---|---|---|---|
| Supply air flow shape | Air diffuser vertical section | - | Laser Melles Griot | - | |

Table 1. Instruments, variables and measurement points and parameters in the experimental setup.

Some experimental tests are carried out in different operational conditions. We impose air mass flow rates ranging between 75 and 250 $m^3$/h. Water temperature between 15 and 18ºC is also forced in the chiller not only to reduce the floor surface temperature as much as possible for handling the cooling load (typically from 20-22ºC), but also to avoid the floor condensation. To give a better understanding of the cooling mode, we run the tests under these environmental conditions. The ambient room temperatures are ranging between 30 and 33ºC. Firstly, we activated the cooling floor in advance due to the high inertia of the self-leveling cement. Afterward, the floor temperature is stabilized, the AHU is activated, and fresh air is supplied to the zone, from 15-22ºC (depending on DV or MV) approximately 10 minutes before the steady-state is reached. This period usually takes between 60 and 90 minutes, depending on the ambient temperature and cooling loads. The objective of these experimental tests is emulating the typical conditions of displacement and mixed ventilation with several temperature differences between supply air and floor surface, checking how it affects to the thermal stratification in the room area and comfort conditions.

*2.2 Theoretical convection heat transfer.*

As Novoselac reported [20], in a room with displacement ventilation, the major heat transfer from room surfaces to the air takes place at the floor surface. Consequently, a precise calculation of convective heat fluxes at the floor is important for accurate predictions of energy consumption, air quality, or thermal comfort.

Spitler et al [21] and Awbi et al. [22] developed convection correlations for determining the convective heat flow, with a methodology based on the conservation of energy at room surfaces, under steady-state heat flow. In both cases, the energy balance on the floor surface is shown as follows:

$$Q_{floor} = Q_{conv} + Q_{rad} \quad , \tag{1}$$

where $Q_{floor}$ is the conductive heat flux in the floor which is equal to the energy removed by the water:

$$Q_{floor} = \dot{m}_w \cdot Cp_w \cdot \left(T_{w,o} - T_{w,i}\right) \quad , \tag{2}$$

and the convective and radiant heat fluxes are the result of the balance with the air and the other surfaces, respectively:

$$Q_{conv} = h_{cv} \cdot A_f \cdot \left(T_z - T_f\right) \ , \tag{3}$$

$$Q_{rad} = h_{rad} \cdot A_f \cdot \left(T_{sup} - T_z\right). \tag{4}$$

The parameters of the energy balance are obtained from experimental data except $h_{rad}$, which is evaluated as 5 W/m$^2$K as Cholewa et al. [23] recommended. Finally, the experimental non-dimensional heat transfer coefficient is determined as follows:

$$Nu_{exp} = \frac{h_{cv}\, D}{k_a} \ , \tag{5}$$

where $k_a$ is the air conductive heat transfer coefficient at the supply temperature and $D$ is the hydraulic diameter of the diffuser.

## 3. Numerical CFD model

### *3.1.Numerical setup*

To solve numerically the flow generated by the diffuser, we have divided the field into two smaller problems. Firstly, we addressed the airflow generated by the rotational diffuser entering the room using as the outlet solution a spherical surface attached to the flow, see Figs. 5 (a) and (b). Secondly, with the results of that simulation we solve the airflow distribution in the room using as the inlet solution for the flow obtained from the previous simulation mapped onto the spherical shell, see Figs. 6 (a) and (b). This numerical methodology has been performed previously in Martinez-Almansa et al. [24], where it was shown an excellent agreement between the numerical solution of the plume generated by the fresh airflow and the experimental smoke visualizations. This numerical methodology allowed us to treat the spatial domains independently, thus

reducing the cost of the numerical simulation due to the details in the geometry to be solved in the vanes of the rotational diffuser, thus avoiding the disparity of cell sizes. Our simulations require two different meshes accordingly: one for the diffuser and other for the room.

We simulated the airflow inside the rotational diffuser using the following spatial domain: we included a cylinder coupled to the rotation diffuser to reproduce the air at the inlet, while the outlet consists of a virtual region. This external spatial domain corresponds to an artificial sphere [see Fig. 5 (a) again]. The height of the cylinder is 300 mm, and the diameter of the sphere is the same as the diffuser. All the meshes have been generated by GAMBIT®. Mainly hexahedra and prisms compose the generated mesh and tetrahedrons are preferred for the region of the vanes. Outlet boundary conditions are set at the sphere, as shown in Fig. 5 (b). Typical mesh sizes are about 4.8 million grid points for the rotational diffuser. Boundary conditions are fixed velocity at the circular surface of the lower part of the cylinder (imposing the flow-rate $Q_{air}$), outlet boundary conditions at the sphere and walls elsewhere. In this first simulation, we have checked that results are independent of temperature, so only velocity and pressure (and turbulence properties) are solved.

(a) (b)

Fig. 5. Rotational diffuser and spatial domain of the simulation (a) and detail of the mesh (b).

Also, a room of 3 m long, 3 m wide and 3 m high was created and meshed with a coarser hexahedral grid, as depicted in Fig. 6. The walls are located far away from the diffuser to reduce the influence of the air supply. The inlet velocity field in the room and other variables such as the temperature or turbulence properties were mapped from the results at the outflow of the rotational diffuser mesh. Typical mesh sizes are about 7.6

million grid points to run the simulations for the room, as shown in Fig. 6 (a). A detail of the surface mesh at the connection of the inlet surface and the isothermal floor is presented in Fig. 6 (b). The maximum skewness is lower than 0.78. We use the supercomputer Picasso at the Supercomputing and Bioinnovation Center at the University of Malaga to carry out the simulations employing 128 cores. Besides, a grid convergence study was performed. To this end, we decreased the characteristic length of the mesh while keeping the same meshing method to reach a final mesh with an increase of 20% in the number of points. Results between the fine and coarse meshes vary less than 1% regarding the velocity field. Boundary conditions are the following. At the sphere, where the fluid enters the room, all the fluid variables (velocity, pressure and turbulent properties) are mapped from the outlet of the diffuser simulation, and a fixed temperature $T_{sup}$ is imposed. The radiant floor is modeled by a non-slip boundary condition and set the temperature on the surface $T_f$. The rest of the walls are considered as outflow.

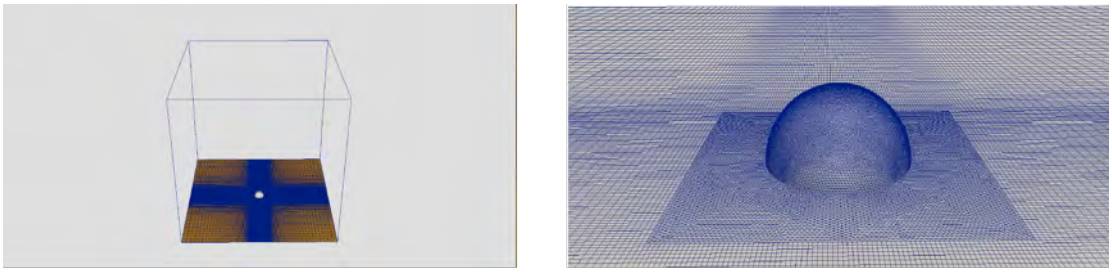

(a) (b)

Fig. 6. Physical space of the room (a) and mesh detail of the room floor near the rotational diffuser (b).

Both problems were solved with OpenFOAM using a turbulent steady-state solver for the diffuser and a Boussinesq turbulent, long-time step unsteady solver for the room. The turbulent model used in this study is the k-ε model, which is a two-equation turbulence model, in which the turbulent viscosity depends on the turbulent kinetic energy k and the turbulent dissipation ε. We show below that there is a good agreement with the experimental data for numerical isothermal ($T_f = T_{sup}$) and non-isothermal ($T_f \neq T_{sup}$) cases.

The non-dimensional parameters that control the problem are the Reynolds number $(Re)$ ,

$$Re = \frac{4 \cdot Q_{air}}{\nu \cdot \pi \cdot D}, \tag{6}$$

where $\nu$ the kinematic viscosity at the supply temperature, and two temperatures ratios defined as follows:

$$\theta_1 = \frac{T_z - T_{sup}}{T_z - T_f}, \qquad \theta_2 = \frac{T_{sup} - 273}{T_z - T_f} \ . \tag{7}$$

To determine the numerical Nusselt number we calculate the heat transfer on the floor $Q_{conv}$ and non-dimensionalize it using the conductive heat transfer coefficient of air at the supply temperature and the diameter:

$$Nu_{num} = \frac{Q_{conv} \cdot D}{k_a \cdot A_f \cdot (T_z - T_f)} \ . \tag{8}$$

## 4. Results.

In this section, the numerical and experimental results are discussed in detail. Firstly, the qualitative structure of the flow for an isothermal problem is studied ($T_f = T_{sup}$). Secondly, a quantitative comparison of the Nusselt number obtained for all the cases studied (isothermal and non-isothermal) is shown. Finally, a new scaling law for the heat transfer coefficient is provided for this system composed by a rotational diffuser coupled with a radiant floor cooling.

### *4.1.Isothermal flow.*

The shape of the plume generated by the rotational floor diffuser is firstly analyzed using smoke visualizations at the room midplane for the isothermal case, in which the following condition is adopted:

$$T_f = T_{sup} = T_z - 6\ K \ . \tag{9}$$

Examples of instantaneous smoke visualizations at two different flow-rates are depicted in Fig. 7, and distances are rendered non-dimensional using the diameter of the diffuser $D$.

The first case represented in Fig. 7 (a) corresponds to an experimental flow-rate of $Q_{air}$ = *75* $m^3/h$. In this case, the weight of the plume, that is denser than the surrounding air, makes the swirling flow reach a given height and then descend to the floor due to buoyancy forces. On the other hand, for higher flow-rates ($Q_{air}$ > *200* $m^3/h$), the flow is mainly directed in the vertical direction ~~reaches the top of the room~~, acting as a mixing ventilation device. The fact of using a swirl diffuser improves mixing at higher distances, so we can state that at lower flow-rates the device acts as a displacement diffuser and at higher flow-rates it behaves as a mixing diffuser.

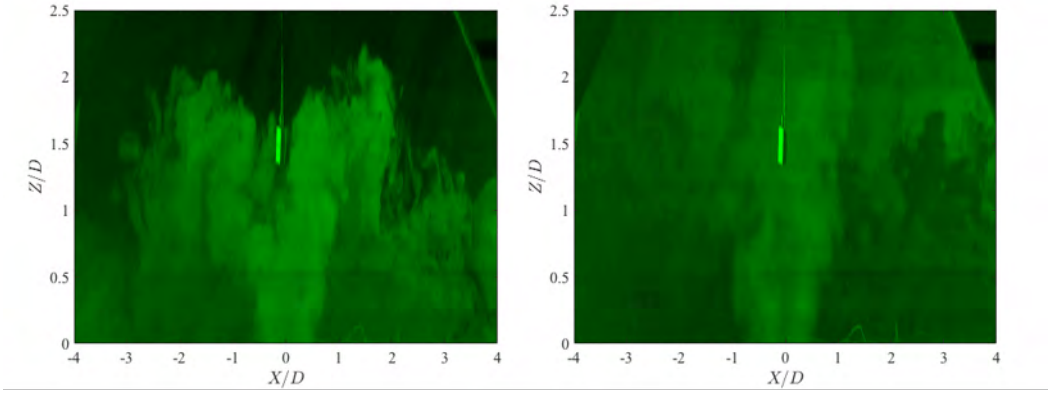


Fig. 7. Instantaneous snapshots of the smoke visualization videos for $Q_{air}$ = 75 $m^3/h$ (a) and $Q_{air}$ = 200 $m^3/h$ (b).

We prove this change in the behavior of the rotational diffuser (DV or MV) by qualitatively comparing the shapes of the smoke plume to those temperatures given by numerical simulations at the midplane. This methodology to compare numerical data to those offered by experimental measurements qualitatively has been already performed in a previous investigation [23], showing qualitatively a good agreement between the isocontours of maximum temperature/intensity of light.

Fig. 8 represents the results for different cases studied: $Q_{air}$ = *75* $m^3/h$ (a)-(b), *150* $m^3/h$ (c)-(d), *200* $m^3/h$ (e)-(f) and *250* $m^3/h$ (g)-(h). It can be observed in this figure that

qualitatively the case with flow-rates below *150 $m^3/h$* has a fountain-type flow pattern, where the flow initially ascends rotating, and due to buoyancy, it descends to the ground. The other cases presented ($Q_{air}$ = *200 $m^3/h$* and *250 $m^3/h$*) have a completely ascending structure in rotation, favoring the mixture with the ambient air. In order to confirm this statement in a more quantitative way, we have compared the ridge lines in both cases [**Height Ridge Computation and Filtering for Visualization, Ronald Peikert ; Filip Sadlo. Conference: Visualization Symposium, 2008. PacificVIS '08. IEEE Pacific (2008)]**, and they have been represented over the numerical results on the left. In this example, it is observed that in cases where the flow is of the fountain type, the rotating jet tends to flow radially, and in this case the buoyancy acts on the flow in such a way that the comparisons of these lines present a fairly good agreement, as was previously verified in [**artículo de Juanjo**]. However, for the case in which the flow is eminently vertical, the numerical temperature field presents the maximum in X/D=0, and nevertheless, the maximum light intensity over the particles presents its maximum in an off-axis position. This is due to the fact that the exact same magnitude is not being compared in both figures (temperature field and light intensity reflected by oil particles), and therefore the thermal diffusivity and the particle diffusivity do not have the same value. In addition, by studying a rotating flow, the particles are more intensely affected by rotation, making their equilibrium position off-axis, due to the centrifugal force.

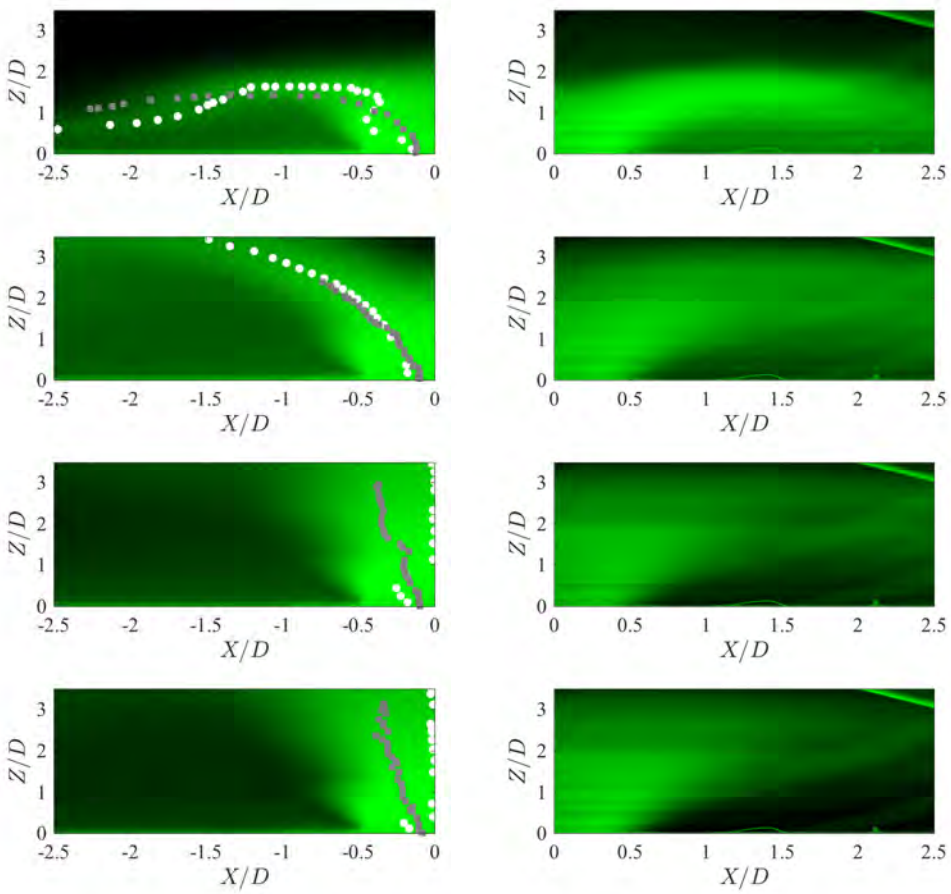


370

371 Fig. 8. Comparison of the experimental smoke plume (right) and numerical contours of
372 temperature at the mid-plane (left) for $Q_{air}$ = 75 $m^3$/h (a)-(b), 150 $m^3$/h (c)-(d), 200 $m^3$/h
373 (e)-(f) and 250 $m^3$/h (g)-(h). On the left, circles represent the ridge line for the
374 temperature and squares for the intensity of light of the particles in the experiments.

375 *4.2.Scaling law.*

376 We perform a comparison of the convective heat transfer coefficient using experimental
377 measurements and numerical results (Eqs. 5 and 7). To that end, we compare the
378 experimental Nusselt number ($Nu_{exp}$) with its numeric counterpart, obtained by
379 simulations with OpenFOAM ($Nu_{num}$). These life-size experiments to provide the
380 values of $Nu_{exp}$ are four hours long, and during this time it is complicated to control
381 outside temperatures since the investigation is carried out inside a building where the
382 temperature cannot be precisely controlled. To provide an accurate comparison of CFD
383 and tests, we have reproduced the experimental cases numerically, using as input

parameters those obtained from the experiments (mainly the flow rate and the measured temperatures on the radiating surface, of the supply air and the ambient air).

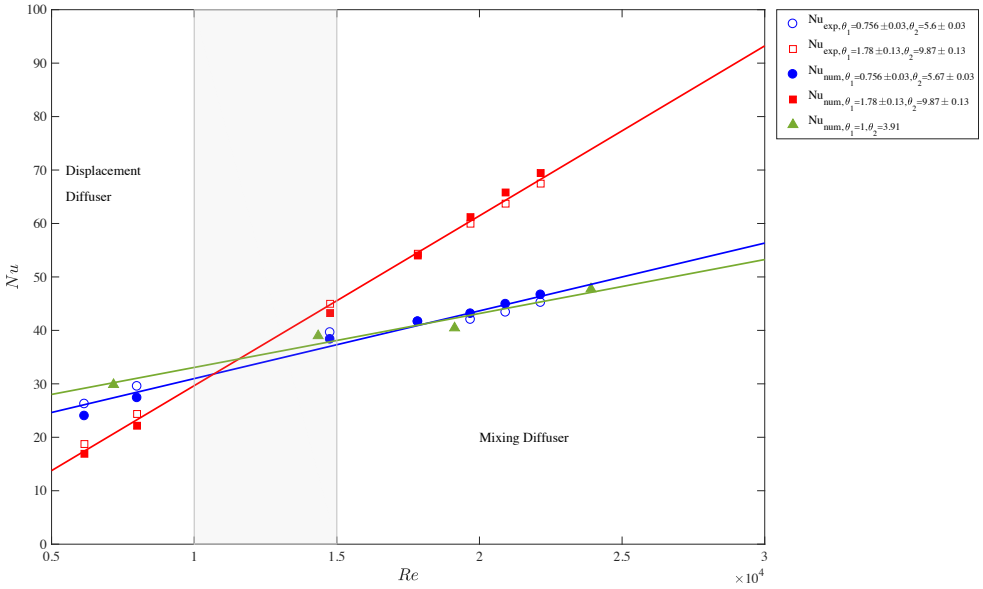


Fig. 9. Comparison of the numerical and experimental non-dimensional value of the heat transfer coefficient versus the Reynolds number for non-isothermal cases (squares for $T_{sup} - T_f \approx -2K$ and circles for $T_{sup} - T_f \approx -3K$). In triangles are shown the results for the isothermal case: $T_{sup} = T_f$ . Filled symbols are used for numerical results and hollow symbols for experimental results.

We depict the results for the non-dimensional heat transfer coefficient in Fig. 9. They include experiments and simulations for the case $T_{sup} - T_f \approx -2\ K$ (in blue) and for case $T_{sup} - T_f \approx -3\ K$ (in red). Besides, we also represent the value of the numerical Nusselt number for the isothermal case $T_f = T_{sup}$ (in green) for the sake of comparison. It can be observed that there is an excellent agreement between the simulations and the experimental results for non-isothermal cases and that the results present an approximately linear trend as a function of the Reynolds number. We marked in the plot with a gray box the estimated area where the change of flow appears following the variation observed in the flow patterns, from DV (fount type) to MV (reaching a great height combined with the ambient air). In any case, we have checked experimentally by visual inspection and numerically by analyzing the velocities, that the rotating jet

flowing out the diffuser does not reach the ceiling of the experimental/numerical room, and it mixes with the ambient air. As an example, for the case of $Q_{air}$=250 $m^3$/h, the maximum height at which we find velocities of the order of v = 0.25 m/s is 1.3 m, less than half the total height of the room. We report that the effect of this change in the structure created by the flow does not change the functional dependence of the heat transfer coefficient appreciably. The correlation coefficient of the linear fit is $R^2$ = 0.9938, showing that the data are very close to the fitted regression line.

For the final application of the results presented in this research, a non-linear fitting has been performed to determine the scaling laws governing the heat transfer in this system, consisting of a radiant floor coupled with a swirl floor diffuser. We make use of the following fitting,

$$Nu_{corr} = a + b\, Re^{c} {\theta_1}^{d} {\theta_2}^{e},$$

where a, b, c, d and e are constants to be determined, for example by using the Nelder-Mead algorithm [ *Nelder, John A.; R. Mead (1965). "A simplex method for function minimization". Computer Journal. 7 (4): 308–313.* ] used for non linear optimization and implemented in Matlab .

$$Re \leq 16000,$$

$$\begin{aligned} Nu_{corr} &= -41.5668 + 4.7499\ Re^{0.3} {\theta_1}^{-0.02} {\theta_2}^{-0.02} \\ &\simeq -41.5668 + 4.7499\ Re^{0.3} \end{aligned} \quad (10)$$

$$Re > 16000,$$

$$Nu_{corr} = 17.1680 + 4.7\ 10^{-5}\ Re^{1.26} {\theta_1}^{0.32} {\theta_2}^{0.46} \quad (11)$$

We depict in Fig. 10 the Nusselt number obtained numerically and experimentally $Nu_{exp,num}$ as a function of the value of the Nusselt number calculated from the correlation (10)-(11). $Nu_{corr}$ The proposed model works reasonably well for values higher than 40 because all points lay on the line $Nu_{corr} = Nu_{exp,num}$~~-, the results are separated from those estimated by the model. This small deviation is because the fresh airflow does not tend to mix with the ambient flow for low Reynolds numbers, and instead of that, it spreads~~

~~on the radiant floor radially forming a typical DV flow pattern~~. Lower values than 40 correspond to Reynolds numbers lower than 16000 ($Q_{air} \approx 175$ m$^3$/h). Again, this critical value indicates that for the temperature values used in this research, the changes in flow patterns are dominated mainly by inertia (Reynolds number), and they depend weakly on temperature differences. We have included the predictions obtained for DV from Novoselak [19] for one isothermal case. This latter point is obtained for a wall diffuser over a flat surface instead of the radial flow of the present research. However, the correlation is valid for forced flow and natural buoyancy-driven flows, since the term regarding the forced flow is multiplied by the factor $T_f - T_{sup}$, so it is zero for the isothermal case. In other words, we compute a heat transfer coefficient associated with DV, even when the supply air and the surface temperature have the same temperature. Hence, the correlation is valid for both DV and MV because DV presents a special pattern flow called "Wall flow" even for an ambient temperature in the room different to the other ones. Nevertheless, the airflow creates a boundary layer for the temperature field, but Reynolds analogy is no longer applicable [16,18].

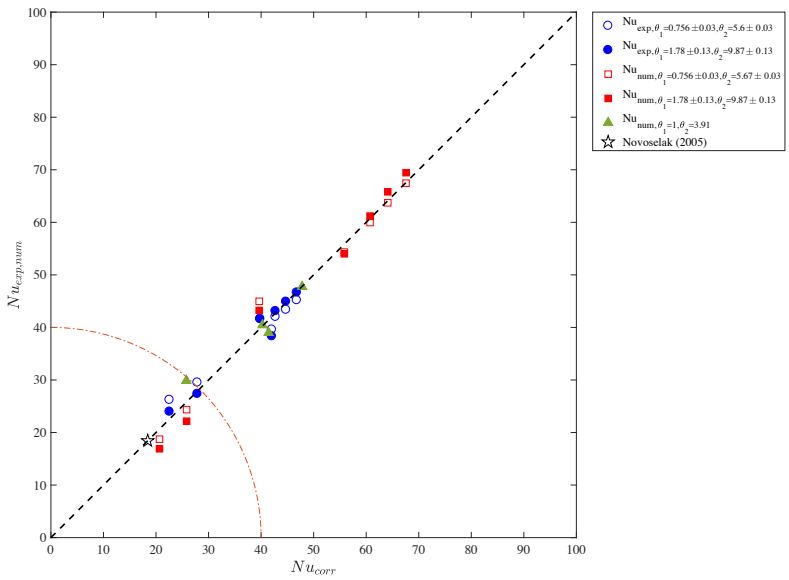


Fig. 10: Comparison of the experimentally and numerically measured Nusselt number vs. the estimation from the correlation presented in eq. (9). The notation is the same as in figure 9. We have marked the perfect correlation with a black dashed line and with a

circular dashed-dotted line the region below which the diffuser acts as a displacement diffuser.

Finally, and to give a better understanding regarding the differences in heat transfer obtained from the different flow configurations produced by the rotational floor diffuser, we have obtained the numerical azimuthal averaged heat transfer for the case of isothermal flow $T_f = T_{sup} = T_z - 6\ K$ and it is shown in Fig. 11 (a). The local Nusselt number is defined as:

$$Nu_r = \frac{Q(r) \cdot D}{k_a \cdot (T_z - T_f)} \ , \tag{12}$$

with $Q(r)$ the local heat flux per unit area defined as:

$$Q(r) = (k_a + k_t)\frac{\partial T}{\partial n} \ , \tag{13}$$

where $n$ is the normal to the radiating floor. This plot indicates that the local Nusselt number has its maximum value near the exit of the diffuser $r/D = 0.5$, decreasing due to the spreading of the flow in the radial direction. There is a change in the structure of $Nu_r$ number as the Reynolds number increases. To check this fact mathematically, we have fitted the local heat transfer by the function

$$Nu_r = A + B \cdot e^{-C \cdot r} \tag{14}$$

The value $C$ of the exponential varies suddenly for $Re \gtrsim 1.510^4$ ($Q_{air} \gtrsim 200\ m^3/h$), in such a way that it can be inferred that for values lower than that critical value, the flow is more oriented towards the ground, thus forming a displacement diffuser, as it has been pointed out previously with the qualitatively comparison of the shape of the plume shown in fig. 8. Conversely, it behaves as a mixing diffuser for higher Reynolds numbers (Fig. 11b).

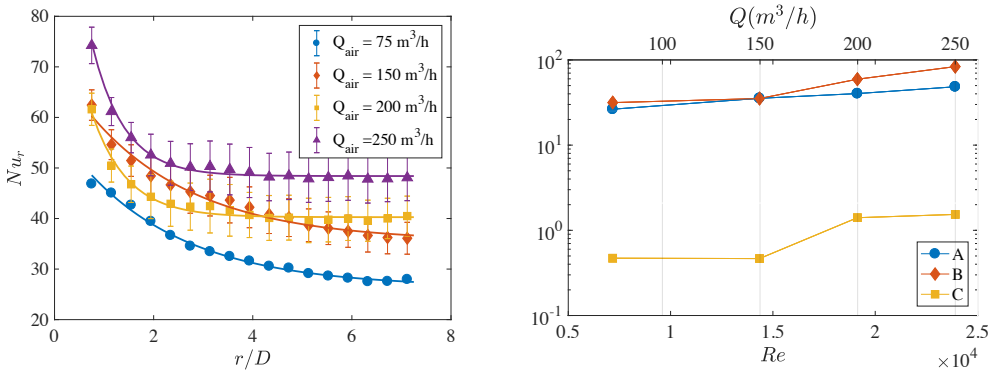


Fig. 11: Azimuthal averaged heat flux as a function of the radial coordinate (a) and parameters for numerical approximation (b) using eq. (14)

## 5. Conclusions.

In this study, we analyze a UFAD system consisting of a radiant floor cooling together with a rotational diffuser both experimentally and numerically. A real-size experiment has been designed, built and instrumented; measuring the operating temperature, the dry temperature at different points, the heat transferred over the floor and the flow rates of supply air for the diffuser and water required by the radiant floor.

For the isothermal case, the plume generated by the flow in the floor diffuser has been qualitatively compared with the numerical results, and in both cases, we proved that the flow patterns present a rotating jet directed upwards (against gravity). This airflow jet can mix with the ambient airflow if it has sufficient inertia, thus acting as a standard air conditioning diffuser. For smaller airflow-rates, the air jet cannot rise, and it falls to the cold floor due to buoyancy-driven forces, thus producing a typical pattern that corresponds to a displacement diffuser. Besides, a quantitative comparison of the dimensionless transfer coefficient (Nu) as function of Reynolds number (Re) has been made for the case in which the supply and floor temperatures are or not equal. The results have provided a reasonably good agreement between experiments and simulations. We detect a change in the slope for Reynolds number ranging between 10000 and 16000 that correspond to a change in the flow patterns observed.

We propose a non-linear fitting of the Nusselt number as a function of the control parameters of the problem, and this fitting works reasonably well for Nusselt number values greater than 40. Small deviations were found for values of Nusselt numbers less than 40. The explanation for these variations is again given using flow visualizations. All the cases for Nu beyond 40 present a different structure in comparison to those observed for values lower than 40, the latter corresponding to a displacement diffuser. The critical value of the Reynolds number is 16000. This value reported makes us believe that, for the temperature difference values used in this investigation, the change from displacement flow to the mixture is fully controlled by inertia, but not on temperature differences. Finally, to double-check the critical Reynolds number and the lack of relationship with the temperature difference, a study of the radial transfer coefficient has been carried out for the isothermal case, and it is observed that it presents a mathematical fitting that changes again suddenly for Re greater than 16000. This fact confirms again that the critical Reynolds number does not depend on how we run the experiment in terms of the temperature differences imposed, so it is not affected by the use of the isothermal or non-isothermal cases.

## Acknowledgement

This research has been financed by CDTI (Spanish Ministry of Economy and Competitiveness) and CTA (Andalucian Technology Corporation) from Spanish Ministry of Economy and Competitiveness. The authors acknowledge this institution for its financial support.

## References

[1] F. Bauman, T. Webster, H. Jin, Design guidelines for underfloor air supply plenums, HPAC Engineering 78 (7) (2006) 28–34.

[2] C. Shen, N. Gao, T. Wang, CFD study on the transmission of indoor pollutants under personalized ventilation, Build. Environ. 63 (2013) 69–78.

[3] M.A. Bos, J.A. Love. A field study of thermal comfort with underfloor air distribution. Building and Environment 69 (2013) 233-240.

[4] G. Kim, L. Schaefer, T.S. Lim, J.T. Kim. Thermal comfort prediction of an underfloor air distribution system in a large indoor environment. Energy and Buildings 64 (2013) 323-331.

[5] S.A. Nada, H.M. El-Batsh, H.F. Elattar, N.M. Ali. CFD investigation of airflow pattern, temperature distribution and thermal comfort of UFAD system for theater buildings applications. Journal of Building Engineering 6 (2016) 274-300.

[6] A. Alajmi, W. El-Amer, Saving energy by using underfloor-air-distribution (UFAD) system in commercial buildings, Energy Convers. Manage. 51 (2010). 1637–1642.

[7] A. Atienza Márquez, J.M. Cejudo López, F. Fernández Hernández, F. Domínguez Muñoz, A. Carrillo Andrés. A comparison of heating terminal units: Fan-coil versus radiant floor, and the combination of both. Energy and Buildings 138 (2017) 621-629.

[8] K.Zhao, X.Liu, Y. Jian. Application of radiant floor cooling in large space buildings – A review. Renewable and Sustainable Energy Reviews 55 (2016) 1083-1096.

[9] F. Fernández Hernández, J.M. Cejudo López, A. Fernández-Gutiérrez, F. Domínguez Muñoz. A new terminal unit combining a radiant floor with an underfloor air system: experimentation and numerical model. Energy and Buildings 133 (2016) 70-78.

[10] A. Atienza Márquez, F. Fernández Hernández, F. Domínguez Muñoz, J.M. Cejudo López. Detailed and simplified models of a terminal unit that combines an UFAD system with a floor cooling. Applied Thermal Engineering 129 (2018) 1079-1091.

[11] K. Zhang, X. Zhang, S. Li, X. Jin. Experimental study on the characteristics of supply air for UFAD system with perforated tiles. Energy and Buildings 80 (2014) 1-6.

[12] P. Raftery, F. Bauman, S. Schiavon, T. Epp. Laboratory testing of a displacement ventilation diffuser for underfloor air distribution systems. Energy and Buildings 108 (2015) 82-91.

546 [13] Y.H. Yau, K.S. Poh, A. Badarudin. A numerical airflow pattern study of a floor
547 swirl diffuser for UFAD system. Energy and Buildings 158 (2018) 525-535.

548 [14] A. Li, X. Wang, Y. Zhang. 2D-PIV experiment analysis on the airflow
549 performance of a floor-based air distribution with a novel mushroom diffuser (FBAD-
550 MD). Energy and Buildings 121 (2016) 114-129.

551 [15] F. Causone, F. Baldin, B. W. Olesen, S.P. Corgnati. Floor heating and cooling
552 combined with displacement ventilation: Possibilities and limitations. Energy and
553 Buildings 42 (2010) 2338-2352.

554 [16] P. Raftery, K.H. Lee, T. Webster, F. Bauman, Performance analysis of an
555 integrated UFAD and radiant hydronic slab system, Appl. Energy 90 (2012)250–257.

556 [17] A. Fernández-Gutiérrez, I. González-Prieto, L. Parras, J.M. Cejudo-López, C. del
557 Pino. Experimental and numerical study of a small-scale and low-velocity indoor
558 diffuser for displacement ventilation: radiant floor cooling coupled. International
559 Journal of Heat and Mass Transfer 87 (2015), 71-78.

560 [18] H. Weller, G. Tabor, H. Jasak, C. Fureby. A tensorial approach to computational
561 continuum mechanics using object-oriented techniques. Computer in Physics, 12
562 (1998), 620-631.

563 [19] A. Fernández-Gutiérrez, I. González-Prieto, L. Parras, P. Gutiérrez-Castillo, J.M.
564 Cejudo-López, C. del Pino. Experimental and numerical study of a small-scale and low-
565 velocity indoor diffuser for displacement ventilation: isothermal floor. Applied Thermal
566 Engineering 87 (2014), 79-88.

567 [20] A. Novoselac, B. J. Burley, J. Srebric. Development of new and validation of
568 existing convection correlations for rooms with displacement ventilation systems.
569 Energy and Buildings 38 (2006), 163-173.

570 [21] J.D. Spitler, C.O. Pedersen, D.E. Fisher, P.F. Menne, J. Cantillo. An experimental
571 facility for investigation of indoor convective heat transfer, ASHRAE Transactions 97
572 (1) (1991), 497–504.

573 [22] H.B. Awbi, A. Hatton, Natural convection from heated room surfaces. Energy and
574 Buildings 30 (1999), 233–244.

[23] T. Cholewa, R. Anasiewicz, A. Siuta-Olcha, M. A. Skwarczynski. On the heat transfer coefficients between heated/cooled radiant ceiling and room. Applied Thermal Engineering 117 (2017) 76-84.

[24] J. J. Martinez-Almansa, A. Fernández-Gutiérrez, L. Parras, C. del Pino. Numerical and experimental study of a HVAC wall diffuser. Building and Environment 80 (2014), 1-10.

## Nomenclature

| | |
|---|---|
| $A_f$ | Surface floor area ($m^2$) |
| $Cp_w$ | Specific heat of the water (J/kg·K) |
| D | Hydraulic diameter of the air diffuser (m) |
| $k_a$ | Thermal conductivity of the air (W/m·K) |
| $h_{cv}$ | Convective heat transfer coefficient ($W/m^2 \cdot K$) |
| $h_{rad}$ | Radiant heat transfer coefficient ($W/m^2 \cdot K$) |
| $m_w$ | Water mass flow rate (kg/s) |
| $Nu_{corr}$ | Correlation Nusselt number |
| $Nu_{exp}$ | Experimental Nusselt number |
| $Nu_{num}$ | Numerical Nusselt number |
| $Q_{air}$ | Volumetric air flow rate ($m^3/s$) |
| $Q_{cv}$ | Convective heat exchange between floor and walls (W) |
| $Q_{floor}$ | Conductive heat flux in the floor (W) |
| $Q_{rad}$ | Radiant heat exchange between floor and walls (W) |
| r | Radial coordinate |
| Re | Reynolds number |

| | |
|---|---|
| $T_f$ | Surface floor temperature (ºC) |
| $T_{sup}$ | Supply air temperature (ºC) |
| $T_{op}$ | Operative air temperature (ºC) |
| $T_{w,i}$ | Inlet water temperature (ºC) |
| $T_{w,o}$ | Outlet water temperature (ºC) |
| $T_{sur}$ | Mean surface air temperature (ºC) |
| $T_z$ | Room air temperature (ºC) |

***Greek letters***

| | |
|---|---|
| $\nu$ | Kinematic viscosity ($m^2/s$) |
| $\theta$ | Non-dimensional temperature |

583